*Rev. Roum. Sci. Techn.– Électrotechn. et Énerg.*
Vol. **68**, *1*, pp. 71–76, Bucarest, 2023

# INDUCTIVE COUPLER FOR BATTERY CHARGING SYSTEM OF HEAVY ELECTRIC VEHICLES

TIBERIU TUDORACHE[1], ANDREI MARINESCU[2], ADRIAN VINTILA[3]

**Keywords: Wireless power transfer; Battery charging of heavy electric vehicles; Finite element analysis; Experimental validation.**

**This paper deals with the numerical analysis of an inductive coupler with double-D coils arrangement for battery charging of heavy electric vehicles. A 3D finite element analysis is used to compute the electromagnetic parameters of the inductive coupler of the wireless power system when the transmitter and the receiver coils are perfectly aligned but also in case of misalignments (misalignments along OX, OY axes as well as rotation around OZ axis and inclination). The transmitter coil is placed on a special magnetic concrete pad inserted into the road and can ensure good magnetic coupling with the receiver coil and high mechanical strength. A ferrite magnetic core backs the receiver coil mounted on the bottom of the vehicle since the wireless power system operates at 85 kHz. The finite element computations are carried out using the professional software package Flux® dedicated to electromagnetic field analysis.**

## 1. INTRODUCTION

The increasing urban pollution generated by the Internal Combustion Engine (ICE) vehicles (cars, vans, buses, trucks, *etc*.) and the growing dependence on depleting fossil fuel reserves contributed to a radical change regarding the public transportation policy in many countries in the last decade [1,2]. One of the solutions agreed upon and implemented in many places consists of electrifying the urban transportation systems, which means gradually replacing the classical vehicles based on ICE with cleaner electric solutions [1,2].

Currently, electric or hybrid cars (EV or PHEV) are part of the everyday urban landscape, allowing the gradual reduction of CO2 pollutant emissions globally [1]. Charging (recharging) the batteries of these vehicles is, at present, almost exclusively carried out by conduction (Plug-In). With the large-scale development of autonomous industrial transport vehicles (AGVs) and autonomous EVs, automatic contactless charging (Wireless) has become the current solution, applicable both to light-duty electric vehicles (LDEVs) and heavy-duty electric vehicles (HDEVs) (especially for city buses, but also for trucks).

Unlike the small power applications [3], the implementation of the wireless power transfer (WPT) solution in heavy vehicles requires much higher charging powers and efficiency, especially in the case of fast/ultra-fast WPT charging systems [2].

In the case of urban electric buses (EBs) that have well-established routes, there are two approaches regarding the increase of the travel distance: buses with high-capacity batteries to cover the entire daily operating time and nighttime charging in the depot practiced on new buses, respectively buses with batteries with lower capacity wirelessly charged on the route or at line ends [4], a preferred method, especially for diesel buses converted to electric buses and called "opportunity charging".

The transition to electric buses is also confirmed in urban regions in Romania. An example is the international workshop [5] organized in Bucharest in 2018 regarding renewing the diesel bus fleet using EBs with zero CO2 emissions.

This paper follows a cycle of Romanian works dedicated to this subject [4,6–8], which refer exclusively to the wireless charging of batteries from EBs, which is currently safe, compact, and efficient. The technical solutions adopted by the precursors [9,10] for the wireless charging of the necessary batteries represent a basis for the standardization of the solutions in the new draft standard SAE J2954/2 [11] intended for HDEV which includes both buses and trucks that appeared under the form of "Recommended Practice" in 2022. It should be noted that SAE J2954/1 [12] and IEC 61980 series [13] already have common practices for LDEVs with wireless charging that have adopted three classes of powers WPT, for: 3.7 kW, 7.7 kW, and 11 kW and three transfer distances Z between transmitter (Tx) and receiver (Rx) coils from 100 mm to 250 mm under conditions of interoperability of systems at a single frequency of 85 kHz with the limitation of the magnetic leakage field level under ICNIRP [14,15] to 27 μH.

HD-WPT symbolizes the power classes in Table 1 from 20 to 500 kW, and the working distances marked with HD Z in Table II are established.

*Table 1*
Power classes in kW for HDEV [11]

| HD-WPT4 | HD-WPT5 | HD-WPT6 | HD-WPT7 | HD-WPT8 | HD-WPT9 |
|---|---|---|---|---|---|
| 20 kW | 50 kW | 75 kW | 150 kW | 250 kW | 500 kW |

*Table 2*
Ground clearance in mm Tx-Rx [11]

| | |
|---|---|
| HD-Z1 | 100-150 mm |
| HD-Z2 | 150-200 mm |
| HD-Z3 | 250-250 mm |

A similar approach is proposed for SAE J2954/2, including the transition of the operating frequency from 22-25 kHz used so far to the frequency of 85 kHz.

The standard also includes a new class of distances for high-powered automatic vehicles for industrial transport (AGV). The transfer distance symbolized by HD-ZM (table III) is small compared to the HD-Z distances in table II.

*Table 3*
Ground clearance in mm Tx-Rx for AGVs [11]

| | |
|---|---|
| HD-ZM1 | 20-40 mm |
| HD-ZM2 | 40-70 mm |
| HD-ZM3 | 70-110 mm |

One can see that currently, the operation parameters of the high-power WPT systems are described with enough details to open the way to the design and implementation of urban EBs with opportunity charging.

This paper is organized as follows: section 2 describes the

[1] "Politehnica" University of Bucharest, Faculty of Electrical Engineering, Spl. Independenţei 313, 060042, Bucharest, E-mail: tiberiu.tudorache@upb.ro
[2] Romanian Technical Science Academy (ASTR) - Craiova Section, Craiova, E-mail: ancor2005@gmail.com
[3] National Institute for Electrical Engineering (ICMET) – Craiova, E-mail: adrian_vintila@icmet.ro

execution of the hybrid inductive coupler with the integration of the Tx coil in the pavement on a support made of Magnetic Concrete (MC) which can withstand the mechanical stress of current urban road traffic. Paragraph 3 is described the numerical model used for electromagnetic field calculations. In sections 4-6, the electromagnetic field of the inductive coupler is treated using the 3D finite element method, the variation of the coupling factor k depending on the distance Tx – Rx for different practical situations, and a comparison with the results obtained on the experimental physical model. The numerical computations are carried out using the professional software package Flux®. The conclusions and the bibliography close the work.

## 2. HIGH-POWER HYBRID INDUCTIVE COUPLER WITH MIMO STRUCTURE

The inductive coupler is the basic component of any WPT system [16]. In the case of EVs and especially in the case of high-power systems, the value of the power transfer efficiency is very important. It must be maintained as constant as possible, regardless of the operating conditions, including the variation of the ground clearance, the mutual positioning of Rx compared to Tx, and the unilateral inclination of the EB for boarding and disembarking passengers in case of opportunity charging on the route. A well-designed WPT system should maintain, at the same time, the leakage magnetic field within limits agreed by ICNIRP [14], *etc*.

This paper deals with the case of an EB from the transferred power class WPT 6, meaning 150 kW and 250 mm maximum ground clearance [11]. At this power level, the classic single Tx-Rx coupler (SISO) cannot be used by simply increasing its dimensions due to the large working distance Z, although the existing space of EB is large enough. Thus, it will be replaced with a MIMO system consisting of two transfer systems with coils in the double D topology with a unitary power of 75 kW placed in line in the EB travel direction, from now on referred to as 2x2 MIMO as shown in [4]. Couplers with a 4x4 or even 6x6 MIMO structure made of identical optimized 2x2 modules can be used for higher power classes. As a result, the structure proposed in work is applicable regardless of the power transferred.

The analyzed inductive coupler was called “hybrid” because Tx is integrated into the pavement and uses an MC structure as a magnetic flux concentrator [6]. Rx uses a classic ferrite structure placed under the EB body. In addition, the dimensions of the two coils, Tx and Rx, are the same because, in the case of urban EB, the route/station positioning is similar. Thus their alignment is more accessible, and a maximum magnetic coupling can be obtained [16]. The modern solution adopted already in large urban regions, which proposes a single lane for buses called Bus Rapid Transit (BRT), solves the above condition by itself [17].

It should be mentioned that until recently, the integration of Tx in the pavement was done using ordinary concrete whose electromagnetic parameters were not of interest to road builders [18, 19]. The spread of WPT equipment has drawn the attention of experts on the poor electromagnetic properties of ordinary concrete that may negatively affect the performance of inductive couplers [20, 21]. It was found that the Tx impedance in the case of concrete has a non-linear increase with frequency. However, ordinary concrete has no magnetic properties (the presence of metal reinforcements is excluded). To avoid the variable influence of ordinary concretes and to eliminate brittle ferrites and finally to stabilize the electromagnetic properties of concrete, MC was used, which includes a certain percentage of soft magnetic particles (ferrites, magnetite, nanocrystalline) [6,7,22–26]. A description of the development process and the method of determining the relative permeability of such a MC is presented in [6]. Relative magnetic permeability μr values between 15 and 35 can be obtained. It was verified by physical experiment and FEM simulation that the dependence of self-inductance versus the relative magnetic permeability of one of the double D coils has a non-linear variation, as shown in Fig. 1.

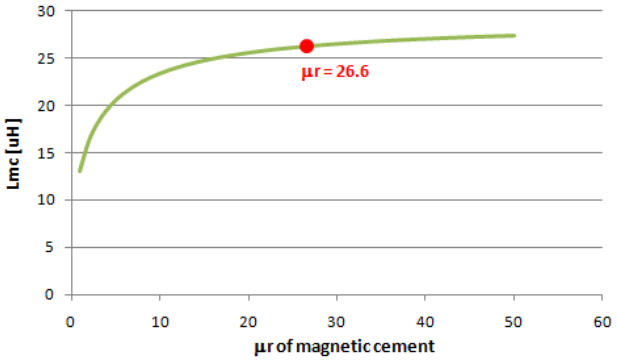


Fig. 1 – Self-inductance of one coil from a double D topology versus relative magnetic permeability $\mu_r$ of MC (3D FE simulation). The experimental value of MC is $\mu_r = 26.6$.

One can notice in Fig. 1 that values above $\mu_r = 30$ do not lead to a significant increase in the inductance. At first glance, these values are small compared to the relative permeability of a good-quality ferrite (>1500). Still, due to the location of the coils in grooves made in the MC plate shown in Fig. 2 and the large distance Z between Tx and Rx, only the magnetic field density in the air is important for the magnetic coupling.

The value $\mu_r = 26.6$ is the relative permeability of the MC used for the Tx pad shown in Fig. 2. This is the Tx structure used for the simulations in the following paragraph.

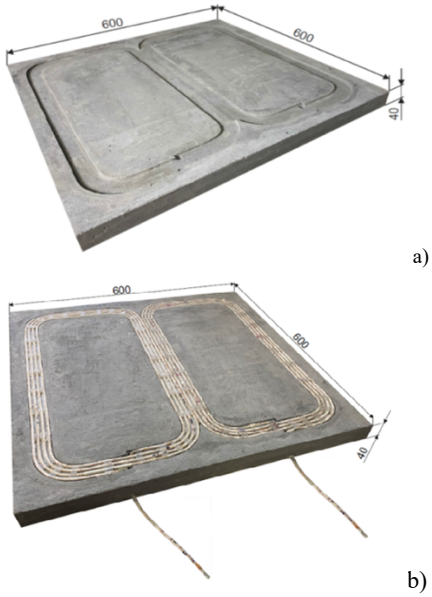


Fig. 2 – MC double D pad scaled-down prototype a) cast structure with grooves for Tx pad; b) Tx coils with 4 turns, 16 mm$^2$ Litz wire connected in series mounted in the MC pad.

Unlike the coupler with non-polarized circular/rectangular coils that generates a vertical magnetic flux, the polarized Double D coupler generates a useful horizontal magnetic flux that, at the same active surface, has a working distance Z of almost twice as much [27].

Due to the high power transferred at 85 kHz frequency [11, 28] through the useful magnetic flux density between Tx and Rx, there is also an important leakage magnetic field.

Besides the fact that the level of the leakage magnetic fields should be limited to 27 μT according to the ICNIRP regulation [14], for EB, not only the leakage magnetic field in the air is important (horizontal component) but also the leakage magnetic fields that enter car body and come directly from the Rx (vertical component). This is a major difference compared to WPT charging of LDEVs since EBs have passengers inside during the opportunity charging process.

The reduction of the leakage magnetic field level that penetrates through the car body can be achieved, for example, by non-magnetic screens.

## 3. FINITE ELEMENT MODEL USED FOR 3D ELECTROMAGNETIC FIELD COMPUTATIONS

A FE numerical analysis was carried out to determine the electromagnetic parameters of the inductive coupler of the studied WPT system in various scenarios.

Due to the geometry structure of the coils (transmitter – Tx and receiver – Rx coils) and their magnetic cores, a 3D FE analysis is required, Fig 3.

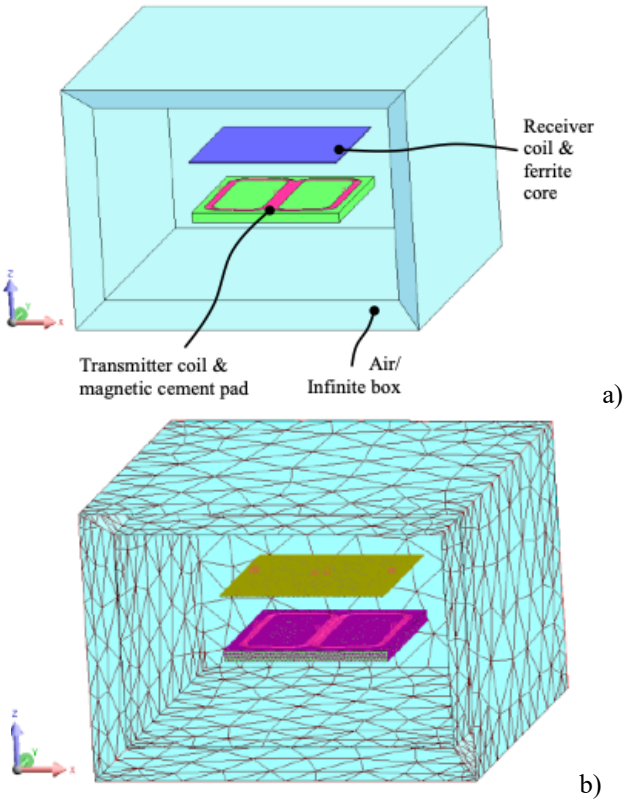


Fig. 3 – Finite element computation domain and FE discretization.

A simplified 2D analysis cannot provide accurate results since the end effects are too significant for such an approach. The 3D computation domain used for the analysis and the FE discretization is shown in Fig. 3. The open boundary to infinity is modeled by an *infinite box*, a Flux® software package feature [29].

The 3D electromagnetic field analysis (ac steady-state magnetic field) is governed by partial differential equations derived from Maxwell's equations, expressed in total Φ and reduced $\Phi_r$ magnetic scalar potentials [29]:

$$\text{curl } \mathbf{H} = \mathbf{J}_s, \tag{1}$$

$$\text{div } \mathbf{B} = 0, \tag{2}$$

$$\text{curl } \mathbf{E} = -\partial\mathbf{B}/\partial t, \tag{3}$$

where **H** stands for the magnetic field strength, $\mathbf{J}_s$ stands for the current density, **B** stands for the magnetic flux density, and **E** stands for the electric field strength.

The relative magnetic permeability of the magnetic concrete was experimentally determined, and its value is 26.6. The ferrite characteristics are initial relative magnetic permeability $\mu_{ri}$ = 2000 and saturation magnetic flux density $B_s$ = 0.5 T.

The electric circuit model associated with the electromagnetic field calculations is shown in Fig. 4.

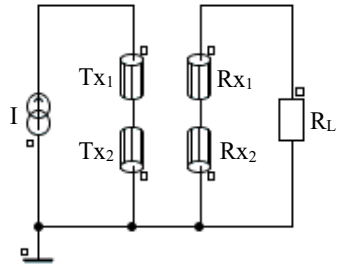


Fig. 4 – Electric circuit model associated with FE analysis.

## 4. NUMERICAL RESULTS. INDUCTIVE COUPLER PARAMETERS

By solving the 3D electromagnetic field problem for the reference coil position (perfectly aligned transmitter and receiver coils), the magnetic flux density distributions on the magnetic concrete pad and the ferrite magnetic core were obtained, Fig. 5.

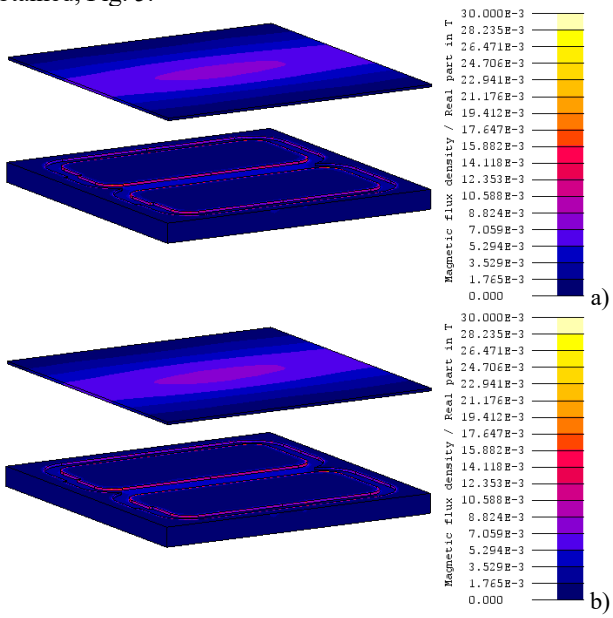


Fig. 5 – Distribution of magnetic flux density on magnetic cores; a) transmitter coil current – 10 A; b) receiver coil current – 10 A.

These results correspond to a current of 10 A applied successively to the transmitter coils Tx (a) and the receiver (Rx

(b). One can notice that the numerical values of the magnetic flux density are well below the saturation levels in both studied cases (and it will remain like that even for a much higher current).

By solving the 3D electromagnetic field problem for different relative distances ($dz$ = 150 - 300 mm) between the transmitter and receiver coils, Fig. 6, the coupling factor values were obtained, Fig. 7. These values vary between approximately 0.26 for 150 mm distance and approximately 0.1 for 250 mm distance.

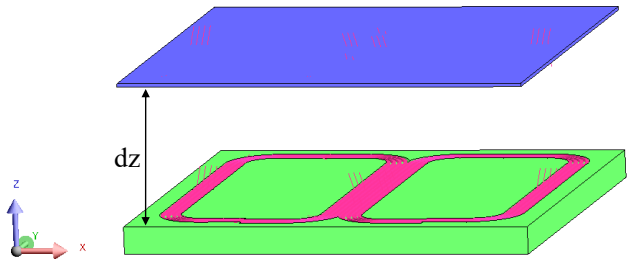


Fig. 6 – Relative distance $dz$ between the transmitter and receiver coils.

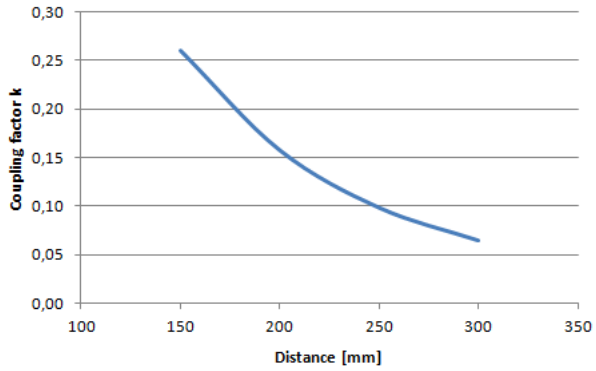


Fig. 7 – Coupling factor $k$ versus distance between transmitter and receiver coils.

## 5. INFLUENCE OF COILS MISALIGNMENT

A perfectly aligned transmitter and receiver coils' positions cannot always be ensured. A smaller or larger misalignment of the coils is very likely. Therefore, the influence of various misalignments (along OX, along OY, rotation around OZ, *etc*.) on the coupling factor is essential.

### 5.1. MISALIGNMENT ALONG OX AXIS

Successive 3D FE numerical simulations were conducted for various misaligned transmitter and receiver coils' positions along the OX axis ($dx \in$ [0 - 200 mm]), Fig. 8.

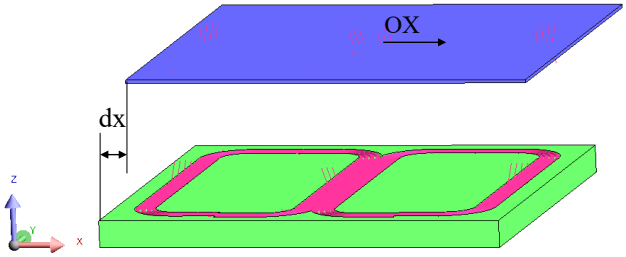


Fig. 8 – Misalignment $dx$ between transmitter and receiver coils.

The numerical results shown in Fig. 9 emphasize the considerable influence of this parameter on the coupling factor. As we can see, it decreases drastically from around 0.16 almost to zero reaching a minimum point followed by a slight increase.

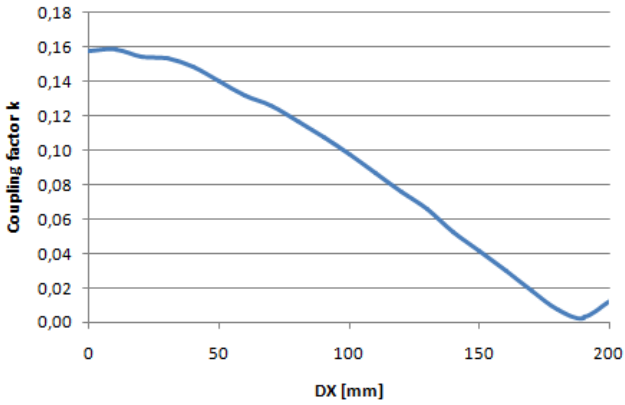


Fig. 9 – Coupling factor $k$ versus misalignment $dx$ between transmitter and receiver coils.

### 5.2. MISALIGNMENT ALONG OY AXIS

The influence of the misaligned positions of transmitter and receiver coils along the OY axis ($dy \in$ [0 - 200 mm]) was also studied by 3D FE numerical simulations, Fig. 10.

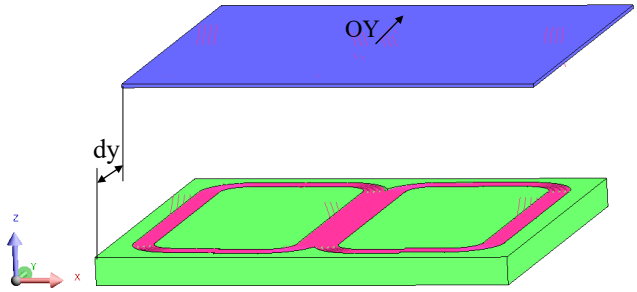


Fig. 10 – Misalignment $dy$ between transmitter and receiver coils.

The numerical results shown in Fig. 11 prove a smaller influence of the misalignment parameter $dy$ on the coupling factor than in the previous case. Here the coupling factor decreases gradually from almost 0.15 down to only 0.11.

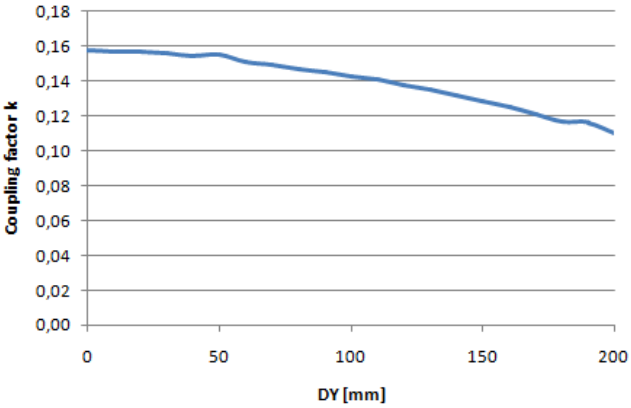


Fig. 11 – Coupling factor $k$ versus misalignment $dy$ between transmitter and receiver coils.

### 5.3. MISALIGNMENT DUE TO ROTATION AROUND OZ AXIS

Another possible misalignment refers to the rotation angle between transmitter and receiver coils around OZ axis ($\alpha z \in$ [0 - 10°]), Fig. 12. The numerical results obtained by 3D FE numerical simulations shown in Fig. 13 prove a negligible influence of the $\alpha z$ angle on the coupling factor between the

transmitter and receiver coils.

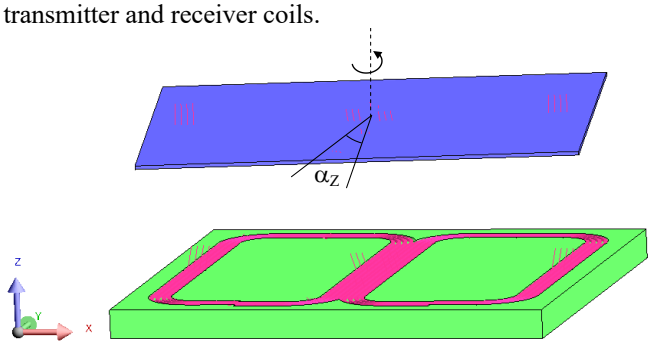


Fig. 12 – Misalignment angle $\alpha_Z$ between transmitter and receiver coils.

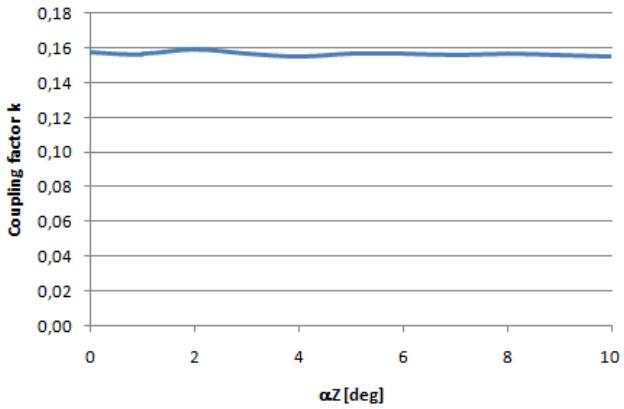


Fig. 13 – Coupling factor *k* versus misalignment angle $\alpha_Z$ between transmitter and receiver coils.

### 5.4. INCLINATION AROUND OY AXIS

Another misalignment may refer to the inclination angle $\alpha_Y$ around the OY axis of the receiver coils concerning the transmitter ones, Fig. 14.

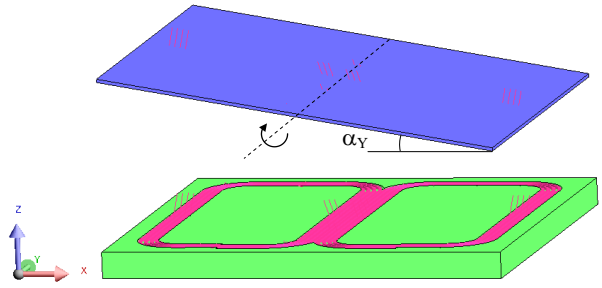


Fig. 14 – Misalignment angle $\alpha_Y$ between transmitter and receiver coils.

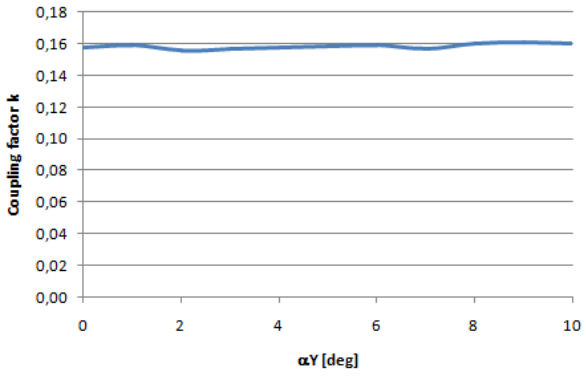


Fig. 15 – Coupling factor *k* versus misalignment angle $\alpha_Y$ between transmitter and receiver coils.

The numerical results obtained by 3D FE simulations for the inclination angle $\alpha_Y \in [0 - 10°]$, prove a negligible influence of this parameter on the coupling factor between the coils, Fig. 15.

## 6. EXPERIMENTAL VALIDATION

In order to validate the computation results obtained by 3D FE analysis, the numerical model presented in section 3 was adapted for the calculation of the self inductance of Tx coils in three scenarios:

- Tx coils in air (without magnetic core - $L_{air}$),
- Tx coils mounted on the MC pad ($L_{mc}$),
- Tx coils in series mounted on the MC pad ($L_{smc}$),

The experimental validation measurements were carried out using the experimental setup shown in Fig. 2.

The numerical results and the experimental ones are presented comparatively in Table IV and a good agreement can be noticed between them. The relative differences in modulus between the results are smaller than 9%.

*Table IV*

Self inductance of Tx coils in air ($L_{air}$), mounted on MC pad ($L_{mc}$) and series connected and mounted on MC pad ($L_{smc}$).

| Inductance | Experiment | | Simulation | Modulus of rel. difference [%] | |
|---|---|---|---|---|---|
| | Coil1 | Coil2 | Coil1/Coil2 | Coil1 | Coil2 |
| $L_{air}$ [µH] | 15.12 | 14.29 | 15.55 | 2.84 | 8.82 |
| $L_{mc}$ [µH] | 24.65 | 25.15 | 26.21 | 6.34 | 4.22 |
| $L_{smc}$ [µH] | 58.15 | | 60.28 | 3.66 | |

The numerical and experimental results presented in Table IV show also that the self inductance of the Tx Double-D arrangement is more than double the inductance of a single Tx coil, which means that the proposed arrangement provides better results in terms of self inductance than two independent Tx coils mounted on magnetic concrete pad.

## 7. CONCLUSIONS

This paper deals with the 3D finite element analysis of an inductive coupler for the battery charging system of heavy electric vehicles. The inductive coupler consists of flat transmitter Tx and receiver Rx coils in double-D arrangement. The magnetic concentrators are made of a special magnetic concrete (with relative magnetic permeability $\mu_r = 26.6$) for the Tx coils and ferrites for the Rx coils.

The numerical analysis was carried out to determine the coupling factor k of the system for various vertical distances between coils (*dz* parameter) and in case of various misalignment types between the coils.

A part of the numerical results was experimentally validated, and the agreement between the numerical simulation results and the experimental ones is very good.

*Received on 31 January 2023*

## REFERENCES

1. N. Golovanov, A. Marinescu, *Electromobility and climate change*, Modern Power Systems (MPS), Cluj-Napoca, Romania (2019).
2. V. Cirimele, R. Torchio, A. Virgillito, F. Freschi, P. Alotto, *Challenges in the electromagnetic modeling of road embedded wireless power transfer*, Energies, **12**, *14*, pp. 2677 (2019).
3. A. Ağçal, O. Vural, *A wireless power transfer system design using transmitter larger than receiver for mobile phones*, Rev. Roum. Sci. Techn – Électrotechn. Et Énerg., **67**, *3*, pp. 359–365 (2022).
4. E. Tudor, A. Marinescu, R. Prejbeanu, A. Vintila, T. Tudorache, D.G. Marinescu, D.O. Neagu, I. Vasile, I.C. Sburlan, *Electric bus*

*platform for urban mobility*, IOP Conf. Series: Earth and Environmental Science, **960**, 012022, IOP Publishing (2022).
5. *** *Workshop on Bus Fleet Renewal through Deployment of Clean and Efficient Vehicles*, Bucharest, 24 April 2018, Available: http://www.jaspersnetwork.org/display/EVE/Bus+fleet+renewal+through+deployment+of+clean+and+efficient+vehicles+-+Bucharest, Accessed: 22.12.2021.
6. A. Marinescu, T. Tudorache, A. Vintila, I. Dumbrava, *A comparative assessment of magnetic concrete versus ferrite for a high power inductive coupler*, Modern Power Systems (MPS), Cluj-Napoca, Romania (2021).
7. A. Marinescu, A. Vintila, T. Tudorache, *Development of a concrete with magnetic properties to improve wireless energy transfer*, International Workshop of Electromagnetic Compatibility (CEM 2020), Sinaia, Romania (2020).
8. A. Marinescu, T. Tudorache, A. Vintilă, *MIMO inductive coupler for high power wireless systems*, Proceedings of SME 2022, Bucharest, Romania (2022).
9. *** Momentum Dynamics, *Wireless charging for electric vehicles*, Available: https://www.momentumdynamics.com/, Accessed: 09-Feb-2019.
10. *** Wave by Ideanomics, *Extend commercial EV range with WAVE high-power wireless charging*, Available: https://waveipt.com/, Accessed: 09.12.2022.
11. ***SAE J2954/2, *Surface Vehicle Information Report*, *Wireless Power Transfer for Heavy-Duty Electric Vehicles* (2022).
12. ***SAE J2954/1, *Surface Vehicle Standard, Wireless Power Transfer for Light-Duty Plug-in/Electric Vehicles and Alignment Methodology* (2020).
13. ***IEC 61980 Part 1, 2, 3, *Electric vehicle wireless power transfer (WPT) systems*.
14.*** ICNIRP, *Guideline for limiting exposure to time-varying electric and magnetic fields (1Hz-100kHz)*, Health Physics, **99**, *6*, pp. 818–836 (2010).
15. A. Marinescu, Mihaela Morega, *Exposure of active medical implants bearers to electromagnetic emissions from wireless power transfer systems*, Rev. Roum. Sci. Techn – Électrotechn. Et Énerg., **67**, *2*, pp. 213–218 (2022).
16. G.A. Covic, J.T. Boys, *Inductive power transfer*, Proc. of the IEEE, **101**, *6*, pp. 1276–1289 (2013).
17. ***FP7 EU ZeEUS Project, *Zero Emission Urban Bus System: Bringing Electrification to the Heart of the Urban Bus Network*, 2013 – 2018, Available: https://zeeus.eu/, Accessed: 10.12.2022.
18. A. Beeldensa, P. Hauspiec, H. Perikd, *Inductive charging through concrete roads: a Belgian case study and application*, 1st European Road Infrastructure Congress, (2016).
19. ****STA Smart Transportation Alliance, Adaptation of Road Infrastructures to the New Mobility*, Technical Report 2 (2019).
20. F. Chen, *Sustainable Implementation of Electrified Roads-Structural and Material Analyses*, Doctoral Thesis, KTH Royal Institute of Technology, Stockholm (2016).
21. V. Cirimele, et al., *Challenges in the Electromagnetic Modeling of Road Embedded Wireless Power Transfer*, Energies, **12**, *14* (2019).
22. H.H. Bache, K.L. Eriksen, *Magnetic cement-bound bodies*, EP0557368B1 Patent, Available: https://patents.google.com/patent/EP0557368B1 (1994).
23. M. Esguerra, R. Lucke, *Application and Production of a Magnetic Product*, US Patent 6,696,638 B2 (2004).
24. R. Tavakoli et al., *Magnetizable concrete composite materials for road-embedded wireless power transfer pads*, IEEE Energy Conversion Congress and Exposition (ECCE), Cincinnati, OH, pp. 4041–4048 (2017).
25. M. Tiemann, M. Clemens, B. Schmuelling, *Comparison of conventional and magnetizable concrete core designs in wireless power transfer for electric vehicles*, EEE PELS Workshop on Emerging Technologies: Wireless Power Transfer (WoW), Seoul, Korea (South), pp. 129–134 (2020).
26. C. Carretero, I. Lope, J. Acero, *Magnetizable concrete flux concentrators for wireless inductive power transfer applications*, IEEE Journal of Emerging and Selected Topics in Power Electronics, **8**, *3*, pp. 2696–2706 (2020).
27. M. Budhia, J. Boys, G. Covic, C.-Y. Huang, *Development of a single sided flux magnetic coupler for electric vehicle IPT charging systems*, IEEE Trans. Ind. Electron., **60**, *1*, pp. 318–328, (2013).
28. S. Park, *Evaluation of Electromagnetic Exposure During 85 kHz Wireless Power Transfer for Electric Vehicles*, IEEE Transactions on Magnetics, **54**, *1*, pp. 1–8, (2018).
29. ****Flux® 9.30. User's guide*, CEDRAT (2006).